Structural Change during Aging and Roasting of Hydrous Ferric Oxide and its Effect on the Adsorption Rate of CO–O_2 Mixture

Ryusaburo FURUICHI, Norio SATO
and Go OKAMOTO*

Faculty of Engineering, Hokkaido University,
Sapporo, Japan

(Received July 10, 1973)

Abstract

The structural change that occurrs during the aging and roasting of hydrous ferric oxide colloid was examined by means of x-ray, DTA, and TGA. The initially amorphous oxide crystallized into α-Fe_2O_3 by aging and by roasting above 300°C, and doping of Cu^{2+} retarded the crystallization of the aging process. The oxide contained three kinds of water, namely, adsorption water, bound water, and crystallization water, and the amount of bound water decreased by extending the aging time and hence by increasing the crystallinity. The effect of this structure change on the reactivity of oxide was studied by examining the consecutive adsorptions of CO–O_2 (mixing ratio = 2 : 1 in volume) and/or CO at 30°C and 100°C. The adsorption kinetics at a constant pressure was found to be of a parabolic type ($V=k_a t^{1/2}$) for 30°C except for the initial period in which Wicke's equation was applied, and Elovich's type ($dV/dt=k\exp(-\alpha V)$) for 100°C. The adsorbed species of 30°C-adsorption was removed completely by outgassing at 100°C, and the species of 100°C-adsorption resulted in the change of the rate parameters (k and α) for the subsequent series of adsorption. These results were discussed with the assumptions that the amorphous oxide provided labile adsorption sites and the amount of bound water represented the amorphous part of the oxide.

1. Introduction

The physico-chemical properties of precipitated transition metal oxides or hydroxides are strongly influenced by the preparation conditions, such as temperature, pH, concentration, kind of salt and alkaline used, aging time, and roasting temperature. In the present study, the effect of the latter two conditions on the reactivity of hydrous ferric oxide was examined. This oxide has been found to change by aging and roasting, from an initially amorphous form to α-Fe_2O_3 crystalline[1]. Generally, amorphous solids have been regarded to be more reactive than well crystallized ones. Moreover, the reactivity of solids has been reported to depend on the nature and the concentration of lattice imperfections[2].

* Present address: Faculty of Science, Science University of Tôkyô, Japan.

Is seems of interest therefore to investigate the change in the reactivity of the oxides with different crystallinities, and the factors determining the reactivity of the amorphous oxide.

It has been observed that the different natural ferric oxides, which are claimed to have the same X-ray structure, exhibited very different catalytic activities against water-gas conversion. The reason for this was attributed to different amounts of water in the catalysts[3]. Shibata and Okamoto[4] observed with the aid of a tritium tracer technique that the passive film on stainless steels containing a large amount of "bound water" was less stable (or more reactive) against corrosion reactions in acid medium as compared with that with a film of a smaller amount of the water. Brenet[5] and Gosh[6] have suggested that the depolarizability of MnO_2 is closely associated with the presence of bound water in the form of OH group and is not necessarily dependent on the X-ray structure of the oxide[7),8]. These studies indicate that the water in oxides or hydroxides plays an important role in their reactivity change. The authors[9] have shown that the amount of bound water in hydrous ferric oxide could be used as a measure for the evaluation of the amount of amorphous part of the oxide and that the dissolution rate of the oxide in acid solutions and the catalytic decomposition of $(N_2H_4)_2H_2SO_4$ by the oxide in alkaline solution were enhanced by increasing the amount of water. In the present paper, the adsorption of CO–O_2 mixture was studied at 30°C and 100°C and the rate was correlated with the amount of bound water and hence with the crystallinity of the oxides, prepared under different aging and roasting conditions.

2. Experimental

Hydrous ferric oxide. *Sample*–1 ; Ferric hydroxide was prepared at 90°C by mixing 54 mℓ of 6N–NH_4OH and 750 mℓ of 0.1 M–$Fe(NO_3)_3$. The pH of the solution containing suspended hydroxide was 9.05. The precipitate obtained was carefully washed and subjected to aging in water at 25°C for various periods of time. After being aged, it was dried at room temperature for 48 hr in a desiccator at pressures of 20 mmHg. The sample to be studied was ground (200 to 300 mesh size) and roasted in air at a fixed heating rate of 10°C/min and kept at given temperatures for 10 min.

Sample–2 ; Ferric oxide containing Cu^{2+} was prepared at 30°C in a similar manner to the above except that 6N–NaOH was used instead of NH_4OH. The amount of 6N–NaOH was adjusted to give a solution of pH=12.5. The procedure for adding Cu^{2+} to the oxide was as follows ; 0.5 M solution of $Cu(NO_3)_2$ was mixed with 50 mℓ of 1.5 M–$Fe(NO_3)_3$ solution. The atomic ratio of $Cu^{2+}/(Fe^{3+}+Cu^{2+})$ was adjusted to desired values. After dilution with water to a volume of 750 mℓ, the hydroxide was precipitated by adding 6N–NaOH. The oxide was aged at 25°C for 15 days in a solution of pH=12.5.

Gases. O_2, CO and He of high purity were supplied from Takachiho Trading Co. **DTA.** DTA was carried out in air by using Al_2O_3 as a reference (Ther-

mofiex 8001 type, Rigaku Denki Co.). The heating rate was 6°C/min. **TGA.** The apparatus used consisted of a quartz spring (sensitivity ; 3.25×10^{-5} g/0.01 mm) and a quartz tube (dia. ; 40 mm) connected to a vacuum system. The weight change was measured in air of 50 mmHg and at a heating rate of 5 °C/min. ***X-ray diffraction.*** The samples were examined by the powder method with FeKα radiation. The diffractometer used was a Geigerflex 2030/p type (Gigaku Denki Co.). ***Specific surface area.*** The surface area of the oxide was estimated by BET method from the amount of adsorbed N_2 at a temperature of liquid nitrogen.

Adsorption of CO–O_2 mixture and CO. The adsorption measurements were carried out by using a conventional constant pressure apparatus, consisting of a gas burette (100 mℓ) and a sample tube The amount of adsorbed gas was measured by reading the volume replaced by mercury in the burette. Prior to a consecutive series of adsorption experiments, the fresh sample (0.3 g) was pumped down at 100°C for 5 hr at 10^{-6} mmHg. After the first series of adsorption measurement, each subsequent series was preceded by an outgassing procedure for 5 hr at the desired temperature and a pressure of 10^{-6} mmHg. Adsorption kinetic data were taken at a pressure of 10 mmHg of CO–O_2 (mixing ratio : 2:1 in volume) or pure CO.

The pre-treatment of fresh oxide with water vapor was made as follows ; the water vapor (11.4 mmHg) was introduced into the sample tube containing the outgassed fresh oxide, and after adsorption of water at 25°C for 5 hr, the sample was evacuated to expell excess water for 3 hr at 30°C. The wet oxide obtained in the above fashion was subjected to consecutive adsorption of the gas. The dead space of sample tube was estimated from the expanded volume of He into the tube, by assuming the ideal gas law.

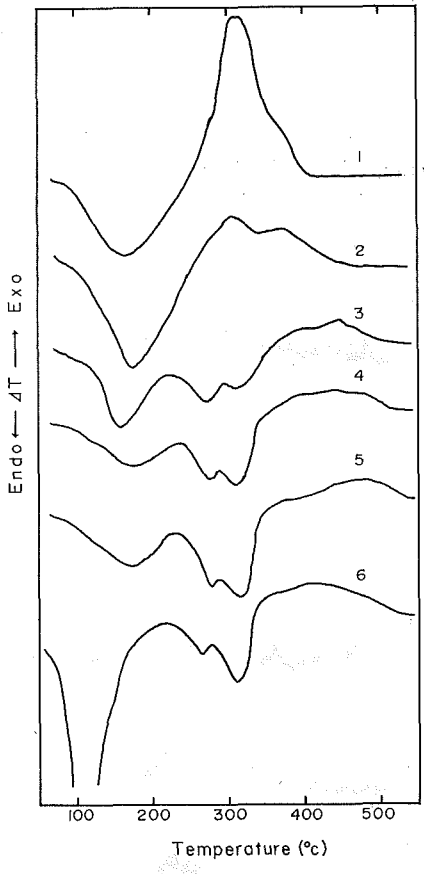

Fig. 1. DTA curves of hydrous ferric oxides (sample–1) aged for, (1):0, (2):7, (3):15, (4):28, and (5):56 days. Curve (6) is the result for water adsorbed oxide aged for 28 days. heating rate:6°C/min, atmosphere:air.

3. Results

DTA, TGA and X-ray diffraction. Fig. 1 shows DTA curves of sample–1 aged for 0, 7, 15, 28, and 56 days. Non-aged oxide shows an endothermic peak at 170°C and an exothermic peak at 300°C. The oxides aged for longer than 15 days show in addition to the peak at 170°C another endothermic peak at

around 300°C. The area of the endothermic peak at 170°C decreases with the increasing aging time, in contrast with the area of endothermic 300°C peak which increases with time of aging. Curve-6 in the figure is a DTA result of the oxide aged for 28 days and then subjected to adsorption of water at 25°C. It may be seen that the adsorbed water gives a large endothermic peak at around 105°C due to dehydration of the adsorbed water, which embeds the endothermic peak at 170°C. The X-ray diffraction patterns of sample-1 showed that non-aged oxide remained amorphous up to 250°C and crystallized into α-Fe_2O_3 at 300°C. This is consistent with the existence of an exothermic DTA peak at 300°C. On the other hand, the oxides aged for longer than 15 days gave diffraction lines of α-Fe_2O_3 when heated up to 110°C and the intensity of them increased with roasting temperature. Accordingly, the endothermic peak at 300°C would correspond to dehydration of the crystallization water in the aged oxide[1]. Sample-2 showed DTA curves similar to those of samples-1. Fig. 2 shows X-ray diffraction patterns of samples-2 roasted at 200°C. It was found that non-aged oxides and aged oxide containing 5%-Cu^{2+} are amorphous, whereas 15 day-aging of the sample without Cu^{2+} results in α-Fe_2O_3 crystalline. These results show that the crystallization is retarded by doping with 5%-Cu^{2+} in the oxide.

The typical TGA curves of samples-2 are shown in Fig. 3, in which non-aged oxide exhibits a continuous smooth curve (Fig. 3-a) and aged oxide indicates a linear part of the curve (Fig. 3-b) at temperatures between 220°C and 300°C.

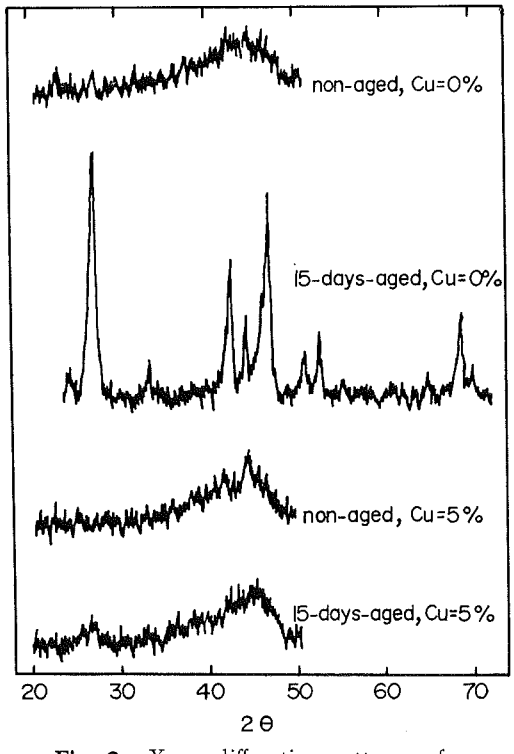

Fig. 2. X-ray diffraction patterns of samples-2 roasted at 200°C.

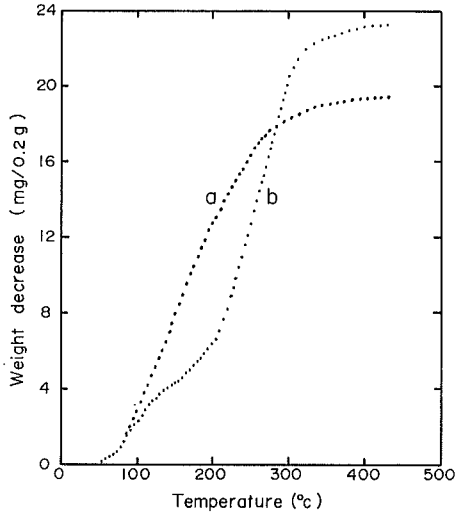

Fig. 3. TGA curves of non-aged and aged oxide (sample-2).
(a): non-aged oxide, Cu^{2+}=0%, (b):15 days aged oxide, Cu^{2+}=0%. heating rate : 5°C/min, atmosphere : air 50 mmHg.

The linear portion was observed for all TGA curves of aged oxides which gave the endothermic DTA peak at 300°C. This suggests that the water released above 220°C is in a different bonding state from that of the water released below this temperature. The weight decrease below 110°C is considered to correspond to the amount of adsorbed water, since the adsorbed water on the oxide was removed below 110°C as shown in Curve-6, Fig. 1. Consequently, the water in hydrous ferric oxide can be classified into three categories; water released by heating in the temperature ranges, (a) lower than than 110°C (adsorption water), (b) between 110°C and 220°C, and (c) higher than 220°C (crystallization water). The second class of the water, henceforth called "bond water", seems to produce the endothermic DTA peak at 170°C and is incorporated into the amorphous part of the oxide. The activation energy of dehydration of the bound water and the crystallization water was evaluated from the rate constants obtained by the isothermal rate measurements at 148–189°C and 249–390°C to be 5.9 kcal/mol for the bound water and 17.1 kcal/mol for the crystallization water, respectively. These activation energies confirm the difference in bonding states of the above.

TABLE 1 Amount of bound water (W_b)

aging time (day)	sample-1					sample-2			
	0	7	15	28	56	15	0	15	15
Cu^{2+} content (%)	—	—	—	—	—	5	0	2	0
amount of bound water (wt %)	5.3	4.7	4.0	3.1	2.9	5.8	5.0	3.1	2.7

TABLE 2 Surface area (S) of the oxides

aging time (day)			sample-1			
			0	15	28	56
roasting temperatue (°C)	110	surface area (m^2/g)	171	139	113	82
	200		165	111	92	90
	250		131	96	79	65
	300		108	79	69	60
	400		42	45	49	47

aging time (day)			sample-2			
			0	2	5	10
Cu^{2+} content (%)			200	200	200	200
roasting temperatur (°C)	0	surface area (m^2/g)	138	155	161	177
	10		59	77	161	179

Table 1 contains the amount of bound water (W_b) evaluated by TGA measurements and Table 2 the surface area of samples-1 and 2.

Rate of adsorption of $CO-O_2$ mixture at 30°C. Figs. 4 and 5 show V-$t^{1/2}$ plots

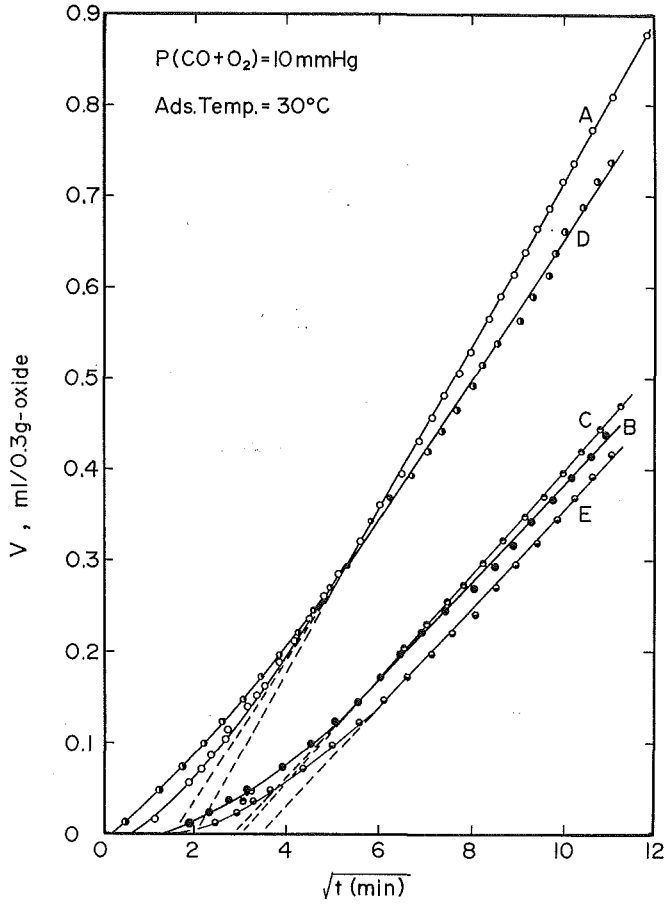

Fig. 4. Five consecutive series of adsorption of CO–O_2 at 30°C.
oxide: sample-1, non-aged, roasted at 200°C,
A: 1-st adsorption on fresh oxide,
B: 2-nd adsorption on oxide outgassed at 30°C after 1-st adsorption,
C: 3-rd at 30°C after 2-nd,
D: 4-th at 100°C after 3-rd,
E: 5-th at 30°C after 4-th.

of data obtained from five consequtive series of adsorption at 30°C for non-aged (sample-1) oxide roasted at 200°C. V is the amount of adsorbed gas, corrected for standard state (mℓ/0.3 g-sample), and t is time in min. The letters from A to E on the curves are arranged in chronological order. Each series of adsorption was preceded by the outgassing procedure at 100°C for Curves A and D, 30°C for Curves B, C, and E in Fig. 4, and at 100°C for Curve C, 30°C for Curves A, B, D, and E in Fig. 5. All V-$t^{1/2}$ plots show straight lines in a range of time longer than $t^{1/2}=5$, which leads to a rate equation (parabolic law);

$$V = k_a t^{1/2} \qquad (1)$$

where k_a is the rate constant and can be estimated from the slope of lines (Table 3).

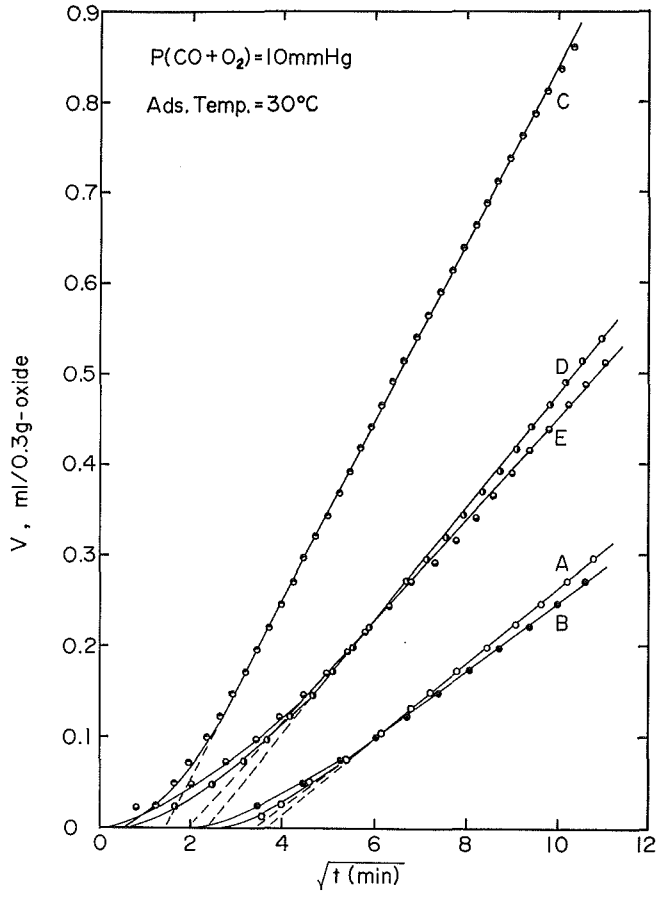

Fig. 5. Five consecutive series of adsorption of CO–O_2 at 30°C on wet oxide.
oxide: sample-1, non-aged, roasted at 200°C, before the measurements water vapour adsorption was made for 5 hr,
A: 1-st adsorption on oxide outgassed at 30°C after water vapour adsorption,
B: 2-nd adsorption on oxide outgassed at 30°C after 1-st adsorption,
C: 3-rd at 100°C after 2-nd,
D: 4-th at 30°C after 3-rd,
E: 5-th at 30°C after 4-th.

TABLE 3 Rate constant (k_a) for CO–O_2 adsorption at 30°C

curve number	$k_a \times 10^2$				
	A	B	C	D	E
dry oxide (Fig. 4)	8.95	5.38	5.69	7.69	5.42
outgassing temp. (°C)	100	30	30	100	30
wet oxide (Fig. 5)	4.13	3.74	9.82	6.22	5.53
outgassing temp. (°C)	30	30	100	30	30

In the case of dry oxide (Fig. 4), the highest k_a is observed in the first series of adsorption on the fresh oxide (Curve A), and k_a of the second and third series (Curves B and C), each being preceded by outgassing at 30°C, have almost the same value, which is approximately two-thirds of the first series. As found from a comparison of Curve D with Curve A, however, an almost complete restoration of the rate is obtained by raising the outgassing temperature up to 100°C from 30°C.

In the case of wet oxide (Fig. 5), the lowest k_a value is obtained in the first and second series of adsorption (Curves A and B) and the highest one results from the third series (Curve C) outgassed at 100°C. Thereafter, the outgassing procedure at 30°C (Curves D and E) maintains the rate at an intermediate value, which is nearly equal to that obtained by corresponding series for dry oxide (Fig. 4, Curves B, C, and E).

The initial part of the adsorption process is not in accord with Eq. (1), as seen in Figs. 4 and 5. Probably, the adsorption mechanism in the initial period of time is different from that in the later period. Here, an assumption was made to the effect that the initial adsorption process attained equilibrium at a time corresponding to the intersection of solid and dotted line shown in the figures. According to the Wicke's rate law[10],

$$\frac{V}{V_e} = 1 - a \exp(-bt), \qquad (2)$$

$\log V_e/(V_e - V)$ was plotted as a function of time as shown in Fig. 6. V_e is defined as the equilibrium amount of adsorption. In the present case, the values of V_e are estimated as the value at the intersectional point.

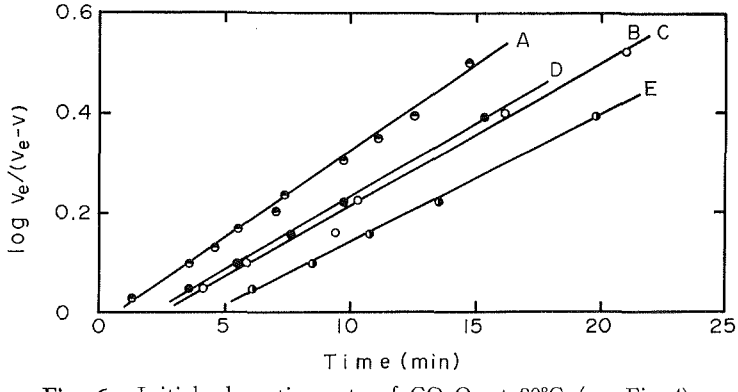

Fig. 6. Initial adsorption rate of CO–O_2 at 30°C (see Fig. 4).

Rate of adsorption of CO–O_2 and CO at 100°C. In Figs. 7 and 8, "linearized" plots of three consecutive series of adsorption of CO–O_2 and CO at 100°C are shown for non-aged oxide (sample-1) roasted at 200°C. Each series is preceded by outgassing at 100°C. Similar results were obtained with wet oxide.

As seen in Figs. 7 and 8, the adsorption at 100°C follows the Elovich's equation[11],

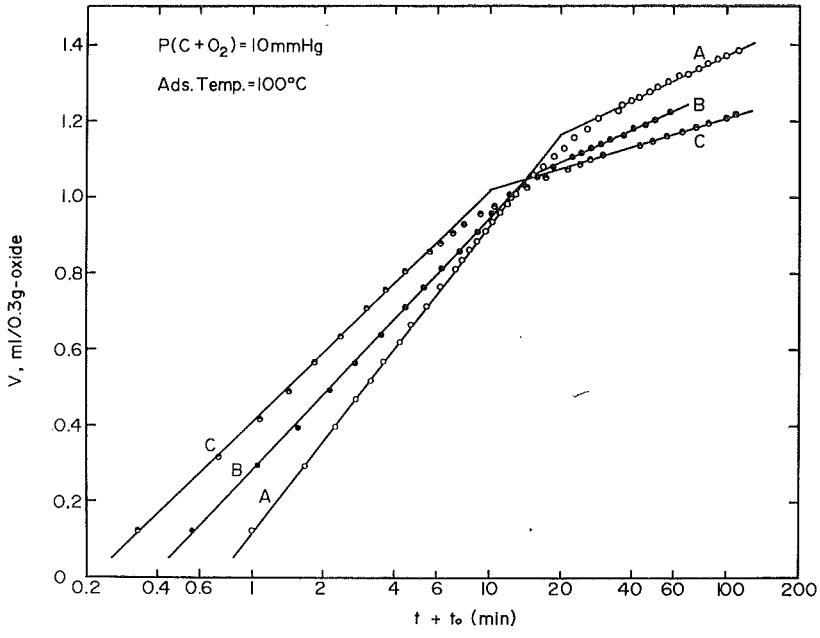

Fig. 7. Three consecutive series of adsorption of CO–O_2 at 100°C.
oxide: sample–1, non-aged, roasted at 200°C,
A: 1-st adsorption on fresh oxide,
B: 2-nd adsorption on oxide outgassed at 100°C after 1-st adsorption,
C: 3-rd at 100°C after 2-nd.

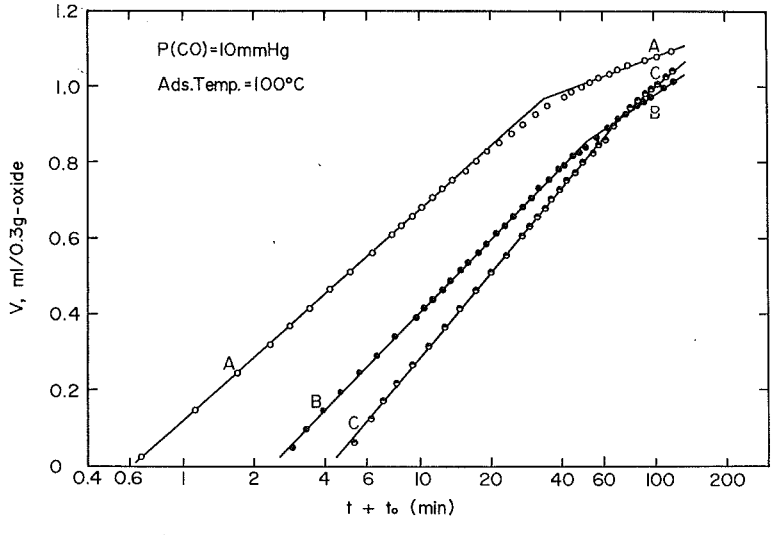

Fig. 8. Three consecutive series of adsorption of CO at 100°C.
oxide: sample–1, non-aged, roasted at 200°C,
A: 1-st adsorption on fresh oxide,
B: 2-nd adsorption on oxide outgassed at 100°C after 1-st adsorption,
C: 3-rd at 100°C after 2-nd.

$$\frac{dV}{dt} = k \exp(-\alpha V) \qquad (3)$$

where k is the initial adsorption rate at $V=0$ and α is a constant. The integrated form of Eq. (3) is,

$$V = \frac{2.303}{\alpha} \log\left(t + \frac{1}{\alpha k}\right) - \frac{2.303}{\alpha} \log \frac{1}{\alpha k} \qquad (4)$$

or

$$V = \frac{2.303}{\alpha} \log(t + t_0) - \frac{2.303}{\alpha} \log t_0 \qquad (5)$$

The value of k and α (thus t_0) can be calculated by using Eq. (4) and the slope of line ($2.303/\alpha$) in the figures. Tables 4 and 5 contain k and α calculated from the data obtained in the early stage of adsorption before an abrupt decrease in the slope of line occurs. It is found that two rate parameters for CO–O_2 adsorption

TABLE 4 Rate parameters in Eq. (3) for CO–O_2 adsorption at 100°C

curve number		A	B	C
dry oxidy (Fig. 7)	α	3.20	3.60	4.15
	k	0.52	0.73	1.05
wet oxide	α	2.88	3.49	3.90
	k	0.49	0.77	1.31

TABLE 5 Rate parameters in Eq. (3) for CO adsorption at 100°C

curve number		A	B	C
dry oxide (Fig. 8)	α	4.35	3.84	3.34
	k	0.55	0.17	0.11
wet oxide	α	4.19	3.66	3.07
	k	0.39	0.12	0.08

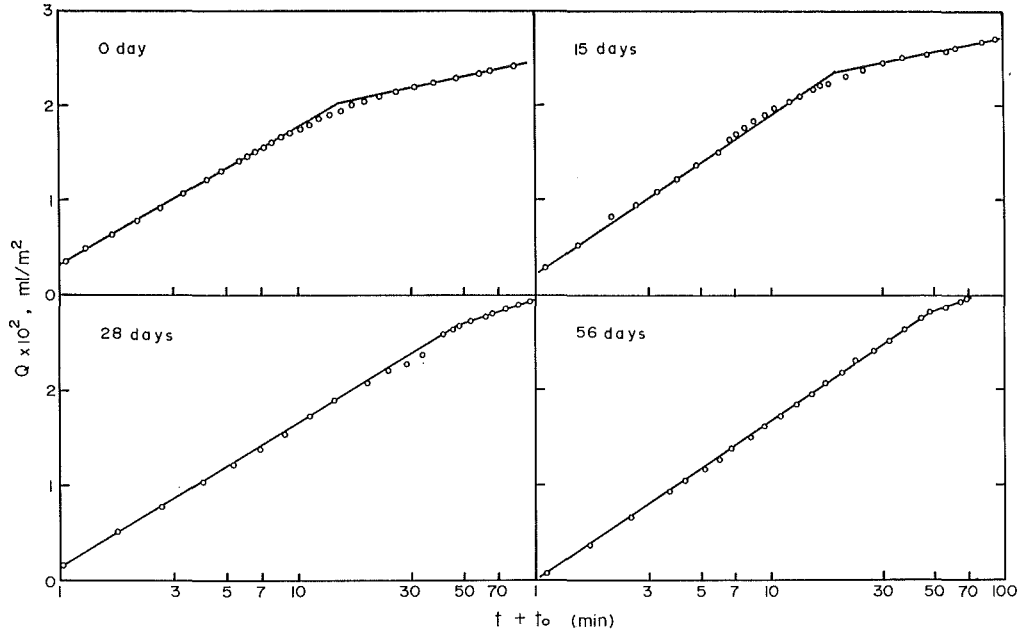

Fig. 9. Effect of aging time on adsorption rate of CO–O_2 at 100°C. oxide: sample-1, roasted at 200°C.

increase progressively from the smallest value for the first series (Curve A) to the largest for the final series (Curve C), in constrast with the reverse trend for CO adsorption. The difference in values of k and α between the dry and the wet oxide is small, which indicates the negligible effect of pre-adsorbed water on the adsorption rate.

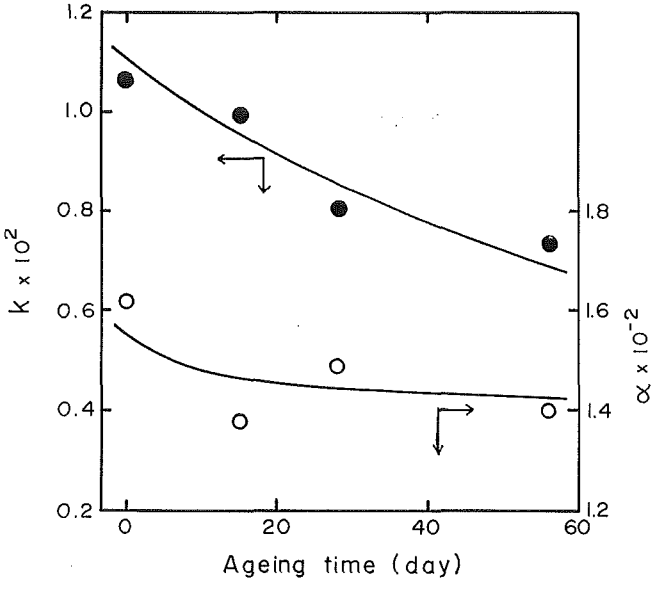

Fig. 10. Change of k and α (Eq. (3)) with aging time.

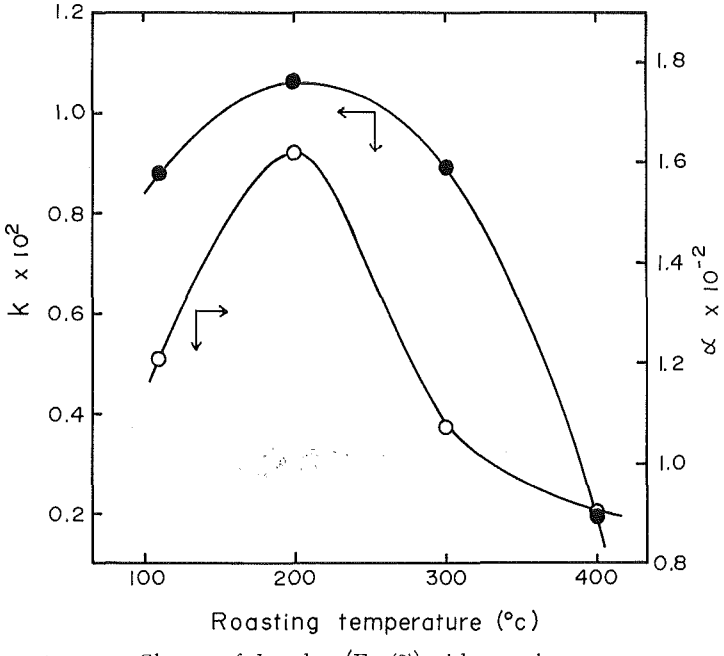

Fig. 11. Change of k and α (Eq. (3)) with roasting temperature.

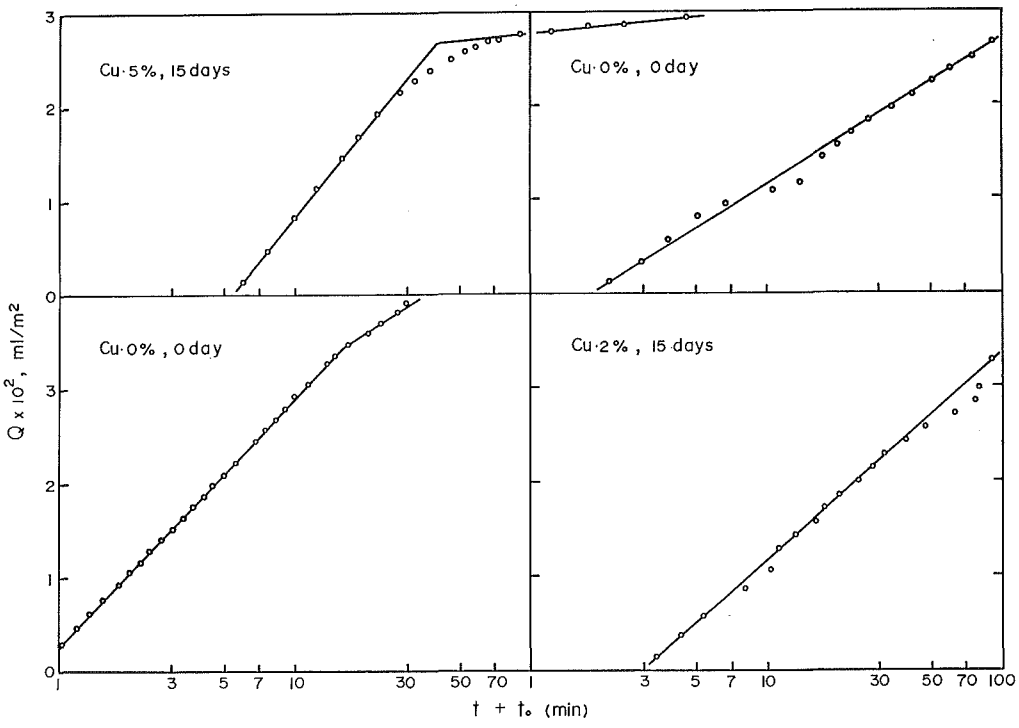

Fig. 12. Rate of adsorption of CO–O_2 on samples–2 at 100°C. oxide: sample–2, roasted at 200°C, pressure: 10 mmHg.

TABLE 6 Rate parameters in Eq. (3) for CO–O_2 adsorption on Cu^{2+}-doped oxide (sample–2) at 100°C

aging time	(day)	15	0	15	15
roasting temp.	(°C)	200	200	200	200
Cu^{2+} content	(%)	5	0	2	0
$k\times10^2$		2.45	1.42	0.32	0.36
$\alpha\times10^2$		0.75	0.87	1.05	1.49

Effect of aging and roasting on the rate of CO–O_2 adsorption. Sample–1 aged for 0, 15, 28, and 56 days, all roasted at 200°C, were subjected to adsorption of CO–O_2 mixture at 100°C. The Elovich's plots of data are shown in Fig. 9, in which the amount of adsorbed gas, denoted by Q (mℓ/m^2), was calculated by using the surface area (S), since the value of S depends on aging time and roasting temperature as shown in Table 2. The rate parameters, k and α, in Eq. (3) estimated from the data are shown in Fig. 10. The effect of roasting temperature on the rate are seen in Fig. 11. It is found that k and α decrease monotonously with time of aging, whereas the maximum value of them is obtained at a roasting temperature of 200°C. The rate parameters for samples–2, containing 0, 2, and 5% of Cu^{2+}, are shown in fig. 12 and Table 6.

4. Discussion

Adsorption at 30°C. The adsorption of CO-O_2 mixture at 30°C was found to be divided into two processes, the initial one obeying Wicke's rate law (Eq. (2)) and the later the parabolic type law (Eq. (1)).

As seen in Table 2, the surface area (S) of the oxide used in this experiment is 165 m^2/g. The apparent density of the oxide was measured pycnometrically with mercury at 25°C to be 4.1 $g/m\ell$. This value leads to 0.22 $m\ell/g$ of pore volume (V_p) by adopting 5.24 $g/m\ell$ as the true density of α-Fe_2O_3[12]. The Knundsen's diffusional flow is generally predominant, when the mean free path of the molecules is greater than the pore diameter (d) of solid[13]. The diameter, d, can be calculated from $d=4V_p/S$ by assuming a cylindorical shape of pores[14]. Substituting numerical values for V_p and S yields $d=270$ Å. The mean free paths of CO and O_2 molecules have been reported to be 584 Å and 647 Å[15], respectively, at 0°C and 1 atm. These values should be much greater at 30°C and 10 mmHg, and indicates that the adsorption at 30°C is rate-determined by the diffusion. The adsorption rate of gas into porous solids has been formulated by the parabolic type equation[16], which is interpreted as follows; the rate is determined by a diffusion process of gaseous molecules into pores of the solids;

$$\frac{V_t - V_0}{V_\infty - V_0} = k_d' t^{1/2} \qquad (6)$$

where k_d' is the rate constant containing the diffusion coefficient, and V_0, V_t and V_∞ are the amount of gas at $t=0$, t, and ∞. In the present experiment, the adsorption capacity, V_∞, can be assumed to be constant, because a single oxide was used, but V_0 is a variable depending on the amount of gas remaining after outgassing. From Eqs. (6) and (1), V and k_d in Eq. (1) are found to correspond to $(V_t - V_\infty)$ and $k_d'(V_\infty - V_0)$, respectively. The first series of adsorption on dry sample (Fig. 4, Curve A) is a case for $V_0=0$. The fact that Curve D in Fig. 4 and Curve C in Fig. 5 shows approximately the same k_d value as Curve A in Fig. 4, may indicate that CO and O_2 and water molecules adsorbed at 30°C were completely removed by the outgassing procedure at 100°C, without leaving any changes in the surface properties of the oxide. The complete removal of adsorbed water at 100°C is consistent with the endothermic DTA peak of the adsorbed water at around 105°C in Curve 6, Fig. 1. This probably means a weak interaction force acting between adsorption site and the adsorbed gas. The small k_d values observed for dry oxides outgassed at 30°C (Fig. 4, Curves C, D, and E) and for wet oxides (Fig. 5, Curves A and B), are considered to show that outgassing at 30°C leads to the incomplete removal of pre-adsorbed species, i.e. $V_0 \neq 0$. The smallest value of k_d obtained by wet oxides would indicate the adsorbed water bonding more strongly with the site than CO and O_2.

The Wicke's rate law, when applied to the initial process of adsorption, is a modification derived from the Langmuir type model[10]. It is considered that, in the initial stage, CO-O_2 adsorbs onto a vacant site on the outer surface of the

oxide particle resulting in giving the rapid establishment of adsorption equilibrium. After completion of the initial adsorption, the rate is determined by diffusion of gas into the pores. The change in the slope and the induction period appearing in Fig. 6 remain uninterpreted.

Adsorption at 100°C. The rate of adsorption of CO–O_2 at 100°C is expressed by the Elovich's equation. This kinetics suggests the chemisorption of the gas at 100°C in contrast with the adsorption at 30°C. The consecutive adsorption resulted in the change of adsorption rate (Figs. 8 and 9); both k and α in Eq. (3) decreased in the case of CO and increased in the case of CO–O_2 mixture, with the number of adsorption series (Tables 4 and 5). This opposite change suggests that the interaction between the site and gas adsorbing on it at 100°C is so strong that the change in the properties of the site is left after the removal of adsorbed gas by the outgassing procedure. These changes in the interaction have been reported by Trapnell[17] on the chemisorption of CO on Cu_2O.

The Elovich's kinetics at constant pressure has been interpreted by two models[18]. The first model assumes that the number of adsorpiton sites (n) on the solid changes with the amount of adsorbed gas (V) according to the equation, $n=n_0 \exp(-aV)$, where "a" is a constant and "n_0" is the number of site at $t=0$. The second model is based on the assumption that the activation energy (E) for chemisorption is allowed for a linear increase with V, that is, $E=E_0+bV$, in which "b" is a constant and "E_0" is the activation energy at $V=0$. The term a is the parameter indicating the number of sites being occupied by a unit volume of adsorbed gas. It is reasonable to assume that this term does not change with the number of adsorption series, since the experiments were carried out under fixed conditions. The term b, which is associated with the change in E, may vary if the properties of the site are changed. Taking into account n and E, the rate of adsorption at 100°C can be formulated as follows;

$$\frac{dV}{dt} = n_0 \exp(-aV)\, k_0 \exp\frac{-(E_0+bV)}{RT} \tag{7}$$

$$= n_0 k_0 \exp\frac{-E_0}{RT} \exp\frac{-(b+aRT)V}{RT} \tag{8}$$

where k_0 is a proportionality constant. From Eqs. (3) and (8), the terms k and α in Eq. (3) are found to correspond to $k_0 n_0 \exp(-E_0/RT)$ and $(b+aRT)/RT$, respectively. The change of α depends only on the term b, since the term a was assumed to be constant, and k depends on the two terms, n_0 and E_0.

The activation energy E is a function of the potential energy of the adsorption site. The stable sites, which have low potential energies, will give large E values, while the labile sites with high potential energies give the small E. Accordingly, the value of b is determined by the heterogeneity or the distribution of potential energy of the sites[19]. That is, if all sites have the same potential energy, the term b will be zero, but if not, a positive value of b will occur, and the lower the potential energy of the site, then the larger the E value. On the basis

of this consideration, the change in α may be interpreted as follows; the increase of α obtained for CO–O_2 adsorption (Table 4) results from an increase in the heterogeneity of the sites with the number of adsorption series, while the decrease for CO adsorption results from a decrease in the heterogeneity. Garner et al.[20] have found that in the case of CO adsorption on Cu_2O, CO molecules adsorbed at 20°C were desorbed as CO, but at elevated adsorption temperatures an increasing fraction of adsorbed gas was desorbed as CO_2. Such abstraction of oxygen atom from the oxide by adsorbed CO has been also observed for NiO[18]. Moreover, Stone[21] has given an order of catalytic activity of metal oxides for the oxidation of CO and showed that Fe_2O_3 acted as one of the most active catalysts among n-type semiconductive oxides at temperatures below 400°C. It is therefore reasonable to assume in the present work that CO adsorbed on hydrous ferric oxide at 100°C desorbs in the form of CO_2 at least in part. Assuming the heterogeneity of the sites and the formation of CO_2 on the labile site, it is considered that the transformation of the labile sites into the stable ones after removal of CO_2 and the narrowspread distribution of potential energy of the sites resulted. These changes will lead to the small value of b in Eq. (7). This is reflected in a decrease of α with by increasing the number of series of CO-adsorption runs (Table 5).

In the case of CO–O_2 adsorption, the sites being deficient in oxygen atom are produced by the formation of CO_2, as in the CO-adsorption, but they are probably occupied again by the adsorption of O_2 in the mixture. This means the re-production of the labile site, such as $Fe_2O_2O_{ad}$, occurs in such a way that it is likely that more labile sites are obtained by the consecutive adsorption-outgassing cycle, which leads to increasing values of b and α (Table 4). The depretive adsorption of O_2 at 100°C was previously observed for hydrous ferric oxide by authors[22], hence it may be said that the re-production of labile sites is a reasonable assumption.

As mentioned before, the initial rate k should depend on both n_0 and E_0. The change in k shown in Tables 4 and 5 can be explained on the basis of above discussion in the following manner; In the case of CO-adsorption, the consecutive adsorption-outgassing cycles at 100°C were assumed to consume the oxygen atom of the labile site which resulted in an increase in E of the site. These changes correspond to the decrease in n_0 and the increase in E_0, thus the decrease of k results. In the case of CO–O_2 adsorption, the adsorption-outgassing cycles were assumed to give re-production of the labile sites by adsorption of O_2. This re-production leads to the lower value of E_0 and unchanged n_0, and thus on to the increase of k. In the present experiments, the adsorption rate of O_2 was not measured, but Winter[23] has reported that the rate for Fe_2O_3 obeyed Elovich's equation at temperatures between 85°C and 250°C.

Effect of aging and roasting on the rate of CO–O_2 adsorption. As shown in Fig. 10, k and α decrease with the lapse of time of aging. The aging caused the crystallization of amorphous oxide as found from DTA and X-ray measurements,

and the amount of the bound water decreased with aging time (Table 1). Therefore it is reasonable to assume that the adsorption sites are located on the amorphous oxide, or that the rate depends on the amount of the amorphous part. Therefore, a progressive decrease in amount of the amorphous part with the aging time results in the corresponding decrease in n_0 or k. The crystallization process of the oxide is the re-arrangement of Fe^{3+} ions and/or O^{2-} ions to give a regular array of them. Thus, as the crystallization proceeds, each adsorption site will take on a similar environmental structure compared with the structure of the amorphous oxide. Therefore, this process can be regarded as the homogenization of the potential energy of the sites, which leads to the decrease in α, since it depends on the term b in Eq. (8).

The amount of bound water (W_b) is expected to be proportional to the amorphous part of the oxide, because the water is contained in the amorphous part as found from DTA, TGA and X-ray experiments. Hence the number of adsorption sites (n_0) can be represented by the value of W_b. In Fig. 13, the values of k obtained from data in Fig. 9 are plotted as a function of W_b for sample-1. The curve should give a linear relation, if E_0 does not change with aging time because $k=k_0 n_0 \exp(-E_0/RT)$. The deviation of experimental curve from the linearity suggests that in addition to the change in n_0, the change in E_0 resulted from the change in crystallinity of the oxide by aging. The slight increase in α in the figure supports this. A similar relation between k and W_b was also found for sample-2 (Tables 1 and 6). This confirms that the labile adsorption sites exist on the amorphous part of the oxide, regardless of whether it contains Cu^{2+} or not.

Fig. 11 shows the convex curve of k and α with a maximum value at a roasting temperature of 200°C.

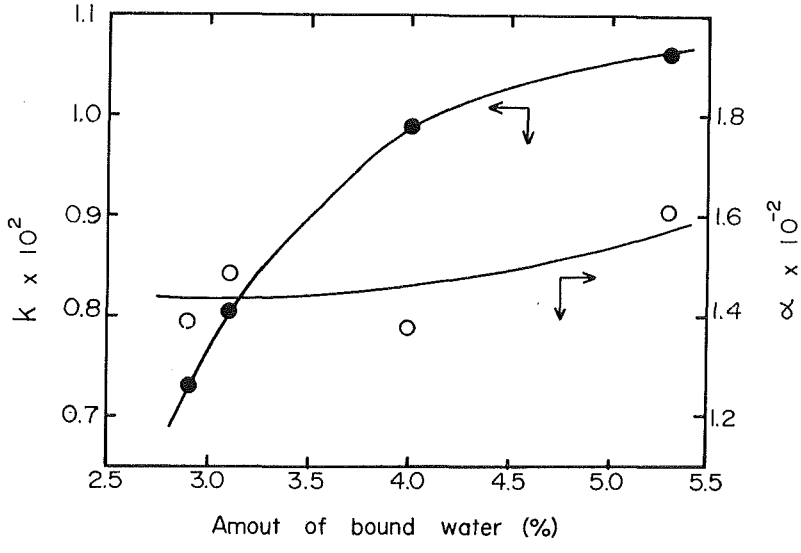

Fig. 13. Relation between rate parameters and amount of bound water in sample-1.

As found from X-ray measurements, non-aged oxide remained amorphous up to 250°C and crystallized into α-Fe_2O_3 at 300°C. Therefore, the decrease in k in a range of roasting temperature between 200 and 400°C is considered to result mainly from a decrease in n_0 due to the crystallization. Moreover, the crystallization causes the homogenization of the E value of the sites, as mentioned before. Thus, the decrease in α resulted in this temperature range. The increase in k and α between 110 and 200°C, however, can not be explained in terms of the crystallization, because the oxide is still amorphous at these temperatures. The difference between the two oxides is that one roasted at 110°C contains bound water, while the other is almost completely dehydrated. The bound water exists in the form of OH, as was confirmed by NMR[24] and magnetic susceptibility measurements[25], which binds ferric ions through hydroxyl bond (OL bridge), such as $\mathrm{Fe{-}\overset{H}{O}{-}Fe}$ or $\mathrm{Fe{<}\overset{OH}{\underset{OH}{}}{>}Fe}$. Therefore, the dehydration at 200°C leads to unstable oxygen bonding (OX bridge). These facts seem to suggest that the roasting at 200°C results in the oxide being in a transitional state just before transforming from the amorphous to the crystalline state. This transitional structure of the oxide is expected to have adsorption sites with low activation energy and enhanced heterogeneity, which lead to the large values of k and α. High reactivity of the structurally transitional oxide has been reported; the maximum reactivity of Fe_2O_3 for the ferrite formation was observed by sintering at 675°C at which the change in the crystallographic modification occurred[26]; the precipitated Cr_2O_3 gel showed maximum catalytic activity for H_2O_2 decomposition, when the gel was roasted at temperatures of 200–300°C at which temperature it transformed from an amorphous state to crystalline[27].

As observed in Figs. 9 and 12, the slope of the Elovich's plot decreased abruptly at the amount of adsorbed gas (Q) of $2\times10^{-2}-3\times10^{-2}$ mℓ/m^2. Assuming that the average cross sectional area of CO-O_2 molecules is 15 Å^2, which was evaluated from 14 Å^2 for O_2 and 16 Å^2 for CO[14], the monolayer adsorption volume is calculated to be 2.5×10^{-2} mℓ/m^2. This is in accordance with the measured Q values at the abrupt change of the slope. The break of the slope has been explained in terms of the change in the properties of adsorption sites[19]. As seen in the figures, the amount of adsorbed gas at the breaking point tends to increase with the increasing crystallinity of the oxide. This indicates that the adsorption on the amorphous oxide is influenced much more readily by the interaction between the adsorbed gas and the sites than the well crystallized oxide surface is.

5. Conclusion

(1) The aging and roasting at 250–300°C of precipitated amorphous hydrous ferric oxides resulted in crystallization into α-Fe_2O_3.

(2) The oxide contains three kinds of water; adsorption water, bound water, and crystallization water. The amount of bound water, which decreases with the aging time, was found to be usable as a parameter indicating the amount of the

amorphous portion of the oxide.

(3) The adsorption rate of CO–O_2 mixture was represented by the parabolic law for 30°C cxcept for the initial period, in which Wicke's law was applied, and by the Elovich's law for 100°C.

(4) Consecutive adsorption-outgassing cycles at 30 and 100°C revealed that the adsorbed species at 30°C was desorbed completely by outgassing at 100°C without leaving any change in properties of the adsorption sites, but the adsorption at 100°C left changes; adsorbed CO was assumed to bind with labile sites and to desorb as CO_2. The formation of CO_2 rendered the sites stable, but this stable site changed to labile one by adsorption of O_2 in the mixture.

(5) The number of adsorption sites and heterogeneity with regard to the potential energy of the sites decreases with time of aging and roasting temperature above 200°C, i.e. with the increase in the crystallinity of the oxide.

(6) The addition of 5%–Cu^{2+} resulted in retarding the crystallization of the oxide induced by the aging. Cu^{2+}–doped sample aged for 15 days showed a comparable amount of bound water and adsorption rate to those of non-aged oxide.

(7) The maximum adsorption rate obtained for the oxide roasted at 200°C was attributed to the resultant transitional structure thereof from the amorphous state to the crystalline.

Acknowledgment. We thank The Matsunaga Foundation for supporting the present work.

6. References

1) Bhattacharyya, S. K., Ramachandran, V. S., and Gosh, J. C.: Advances in Catalysis, **9**, 114 (1957).
2) Reactivity of Solids (J. H. DeBoer, ed.) Elsevier, London (1961), (G. M. Schwab, ed.) Elsevier, London (1965).
3) Takahashi, T., Thesis, Hokkaido Univ. (1965).
4) Shibata, T. and Okamoto, G., Nature, 1350 (1965), 3-rd International Congress of Metallic Corrosion (1966).
5) Brenet, J. P., Batteries, p. 357, Pargamon, London (1963).
6) Gosh, S., J. Electrochem. Soc. Japan, **34**, 38 (1966).
7) Brenet, J. P., C. A. Acad. Sci., **246**, 2469 (1958).
8) Fukuda, M., J. Electrochem. Soc. Japan, **28**, 67 (1960).
9) Furuichi, R., Sato, N. and Okamoto, G., Kogyo Kagaku Zasshi (J. Chem. Soc. Japan), **68**, 1178 (1965), **69**, 1010 (1966).
10) Wicke, E., Kolloid Z., **86**, 167 (1937).
11) Rozinsky, S. Z., and Zeldovich, J., J. Acta Physcochim. (USSR), **1**, 554 (1934).
12) "Handbook of Chemistry and Physics", 51st ed., p. B-99, The Chemical Rubber Co., Cleveland, Ohio (1971).
13) Thomas, J. M., and Thomas, W. J., in "Introduction to the Principles of Heterogeneous Catalysis", p. 231, Academic Press (1967).
14) Dallavalle, J. M., in "Fine Particle Measurements", Macmillan, New York (1959).
15) Moor, W. J., in "Physical Chemisry", 3-rd ed., Prentice-Hall (1962).
16) Barrer, R. M., and Ibbitson, D. A., Trans. Faraday Soc., **40**, 206 (1944).
17) Trapnell, B. M. W., in "Chemisorption", p. 191, Butterworths (1955).

18) Peers, A. M., J. Catal., **4,** 672 (1965).
19) Low, M. J. D., Chem. Rev., **60,** 267 (1960).
20) Garner, W. E., Gray, J. J., and Stone, F. S., Disc. Faraday Soc., **8,** 246 (1950).
21) Stone, F. S., in "Chemistry of Solid State", ed. by Garner, p. 397, Butterworths, London (1955).
22) Furuichi, R., Sato, N., and Okamoto, G., Bull. Facut. Eng. Hokkaido Univ., No. 56, p. 87 (1970).
23) Winter, E. R. S., J. Chem. Soc., 3824 (1955).
24) Okamoto, G., Euruichi, R., and Sato, N., Electrochim. Acta, **12,** 1287 (1967).
25) Mulay, L. N., and Naylor, M. C., in "Advances in the Chemistry of Co-ordination Compounds", p. 520, Macmillan, New York (1961).
26) Solymosi, F., Laky, K., and Szabo, Z. G., Z. anorg. Allg. Chem., **368,** 211 (1969).
27) Burzyk, J., Deren, J., and Haber, J., in "Reactivity of Solids", ed. by Schwab, G. M., p. 468, Elsevier (1965).